Metamaterial-Based Dispersion Engineering to Achieve High Fidelity Output Pulses From a Log-Periodic Dipole Array

Richard W. Ziolkowski, *Fellow, IEEE*, and Peng Jin, *Student Member, IEEE*

***Abstract*—A metamaterial-enabled approach is presented that allows one to engineer the dispersion of a log-periodic dipole array antenna (LPDA) to make it more suitable for wide bandwidth pulse transmission. By modifying the LPDA with electrically small transmission line metamaterial-based negative and positive phase shifters, the phase of each element of the LPDA are adjusted such that in the main beam direction, the phase shifts between each element approximates a linear phase variation. The performance characteristics of the resulting dispersion-engineered LPDA are obtained numerically with HFSS and MATLAB simulations. By measuring in the far field the fidelity between the actual transmitted pulse and the idealized output waveform, the required component values of the phase shifters are optimized. Significant improvements in the fidelity of the pulses transmitted are demonstrated with eight and ten element LPDAs.**

***Index Terms*—Antenna theory, antenna transient analysis, log periodic antennas, metamaterials, phase shifters.**

I. Introduction

With the recent interest in ultrawide bandwidth (UWB) systems for communications applications, there has been a surge of interest in UWB antennas. These systems use UWB pulses rather than narrow bandwidth signals to propagate the information. Unfortunately, the log-periodic dipole array (LPDA) antenna, which is well-known for wide bandwidth applications, is not suitable for these pulsed applications. Because of the frequency dependent phase shifts that exist between the elements of this antenna, the log-periodic array is known to be a very dispersive environment for a pulsed excitation; and, consequently, its output signal is a severely distorted version of the input pulse. While there have been many novel antenna designs introduced to satisfy UWB application criteria, the prevalence, simplicity and familiarity of the log-periodic array would make it an appealing choice if one could suggest a means to overcome these phase shift issues with properly centered phases.

In this paper we consider transmission line-based metamaterials (MTMs) to achieve the appropriate phase shift elements and their introduction into a log-periodic array to correct for the detrimental phase shifts associated with it. This idea was introduced in [1]. We report data to support the fact that this approach leads to a modified log-periodic array that has a sufficiently flat spectral response over a wide frequency band and that produces the requisite phase values at the dominant frequencies to achieve time alignment of the output signals to achieve an overall high fidelity output pulse. Moreover, the design is straightforward and suggests the possibility of retrofitting existing log-periodic systems to take advantage of this MTM technology. Consequently, this dispersion-engineered log-periodic array may have an important impact on UWB system designs and applications.

Manuscript received June 05, 2007; revised May 24, 2008. Current version published December 30, 2008. This work was supported in part by DARPA under Contract HR0011-05-C-0068 and in part by Los Alamos National Laboratory under Contract 49124-001-07.

The authors are with the Department of Electrical and Computer Engineering, University of Arizona, Tucson, AZ 85721-0104 USA (e-mail: ziolkowski@ece.arizona.edu; pjin@ece.arizona.edu).

Color versions of one or more of the figures in this paper are available online at http://ieeexplore.ieee.org.

Digital Object Identifier 10.1109/TAP.2008.2007277

II. LPDA Antenna Dispersion

To demonstrate the frequency dispersion observed in the output pulses generated by an LPDA antenna, we adopt the differentiated Gaussian pulse as the waveform that is used to excite the current sources driving the LPDA elements. This bipolar pulse waveform is shown in Fig. 1(a); it removes the DC components from the input spectrum as shown in in Fig. 1(b). Because its behavior can be treated analytically, we also adopt an infinitesimal electric dipole as our basic time domain reference antenna. It has a highly capacitive nature and, as a result, the far zone electric field generated by this infinitesimal dipole antenna is proportional to the time derivative of the current pulse that excites it. While an infinitesimal dipole can thus radiate theoretically all of the frequencies in the bipolar pulse driving it, it must be noted that, in practice, it is extremely electrically small and can not be matched directly to a real source over a wide range of frequencies. Nonetheless, because one can calculate its far field response with little difficulty, it provides an efficient analytical means of representing the overall time domain response of an LPDA, which can be matched to a realistic source over a wide range of frequencies.

For demonstration purposes only, we assume the frequency range of interest in this paper to be covered by the LPDA antenna is $1\ \text{GHz} \leq f \leq 4\ \text{GHz}$. For the purpose of performing frequency domain ANSOFT High Frequency Structure Simulator (HFSS) and MATLAB simulations, we band-limit the actual excitation pulse to that frequency range. To illustrate the form of the electric field radiated by a broadband antenna driven with such a band limited bipolar pulse, the electric field signal radiated into the far field by the infinitesimal dipole antenna was calculated. This signal is shown in Fig. 2, normalized by its total output power. A diagram of the log-periodic printed-dipole

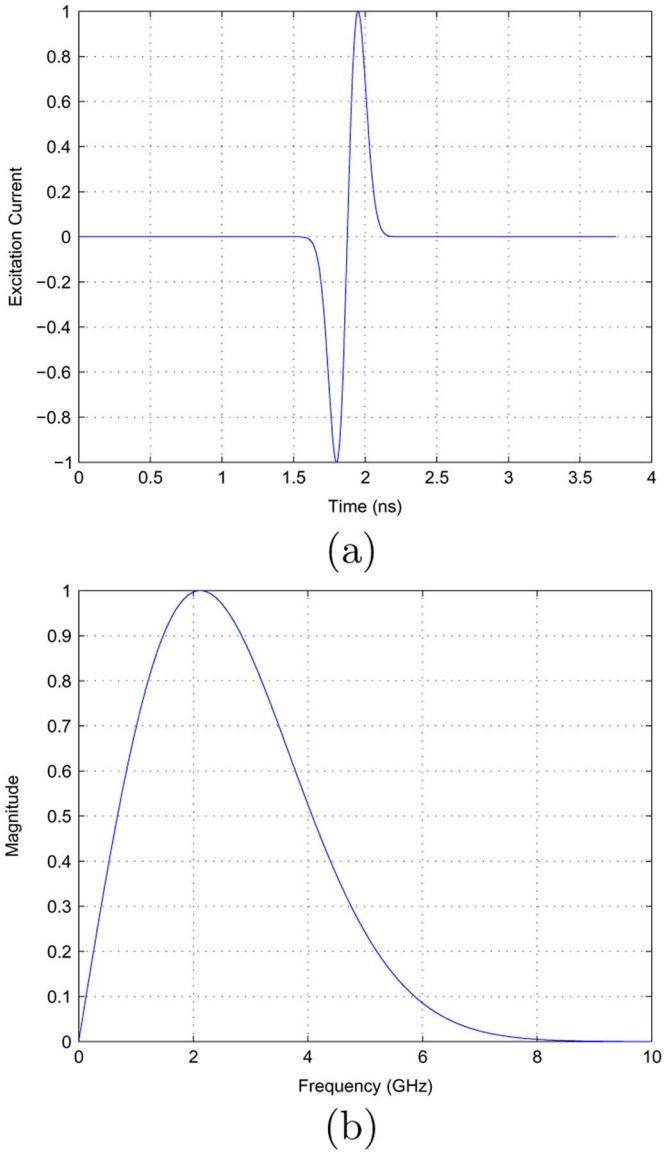

Fig. 1. Current source excitation: (a) Bipolar pulse time history, (b) bipolar pulse spectrum.

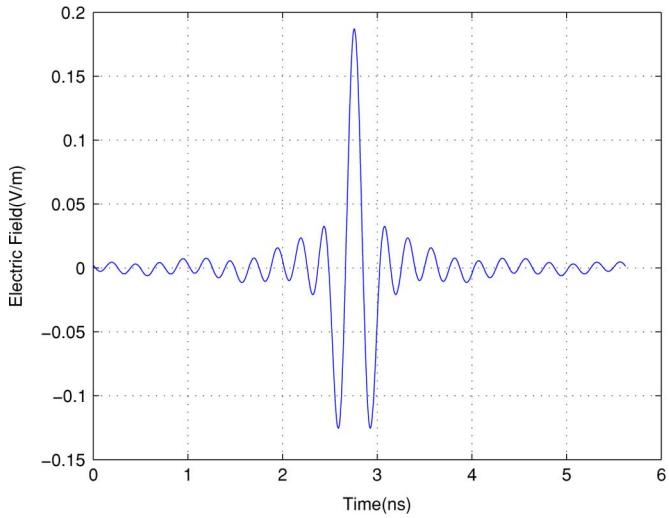

Fig. 2. Far zone electric field radiated by an infinitesimal dipole that is driven with a band-limited version of the source excitation pulse shown in Fig. 1(a).

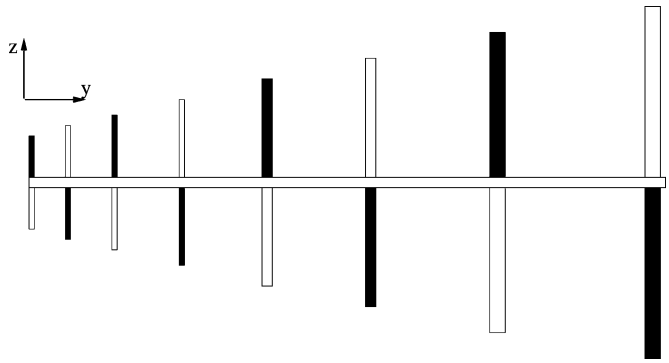

Fig. 3. Printed log-periodic dipole array geometry.

array antenna [2] considered in this paper is shown in Fig. 3. A standard crisscross connection was assumed and implemented with a two parallel layer structure that is represented in Fig. 3 by the black and white colors. This LPDA antenna is assumed to be located in the $x = 0$ plane; its dipole elements are oriented parallel to z axis with the largest element being the furthest away from the origin along the $+\hat{y}$ direction.

To begin, an eight-element log-periodic printed dipole antenna was analyzed analytically with MATLAB using the circuit model given in [3] and numerically with HFSS for the indicated $1\ \text{GHz} \leq f \leq 4\ \text{GHz}$ frequency range. The HFSS predicted S_{11} values are shown in Fig. 4(a). The return losses are well below -10 dB throughout the frequency band of interest. The feed point current $I_{f,n}$ induced on each printed dipole in the LPDA antenna was measured using the HFSS Fields Calculator, where n denotes the nth dipole and f denotes the frequency. For each current $I_{f,n}$, the far zone electric fields can be calculated with the expression [4]

$$E_\theta \simeq j\eta I_{f,n}\frac{e^{-jkr_n}}{4\pi r_n}\left[2\frac{\cos\left(\frac{kh_n}{2}\cos\theta\right)-\cos\frac{kh_n}{2}}{\sin\theta}\right]\times\left[\frac{1}{\sin\left(\frac{kh_n}{2}\right)}\right] \quad (1)$$

where h_n is the length of the nth dipole and r_n is the physical distance between the nth dipole and the observation point. With this expression the far zone electric field resulting from each individual element in the array is obtained at a specified observation point for a single frequency value. The total far zone electric field is then obtained as the superposition of all of these individual far zone electric fields. To obtain the time domain signal observed at that far field point, this frequency domain calculation is repeated for enough frequency points to resolve the frequency interval of interest and an inverse Fourier transform is applied to all of these results. It should be noted that for the nth radiating element, which has the length h_n, the electric field component $|E_\theta|$ at the frequency f is affected by $|I_{f,n}|$ and f itself. We choose the frequency f_n at which $|E_\theta|$ is maximized

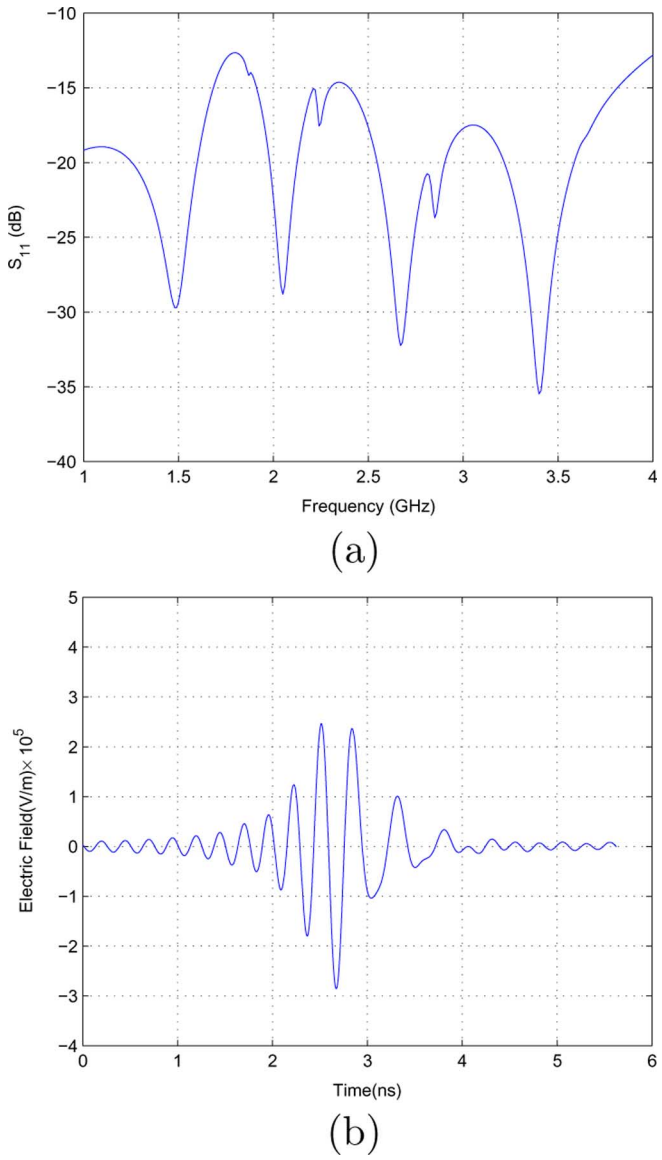

Fig. 4. Log-periodic dipole array response: (a) S_{11} and (b) far-zone electric field.

as the dominant frequency of the nth element. Based on the currents predicted by the HFSS simulations, the far zone electric field radiated by the eight element log-periodic antenna illustrated in Fig. 3 is shown in Fig. 4(b) for $\theta = \pi/2, \phi = 3\pi/2$. Compared with the waveform in Fig. 2, the effects of frequency dispersion introduced by the LPDA antenna are readily observed. We note that it was found to be necessary to calculate the far field with the indicated combined analytical-numerical approach because a calculation with HFSS alone was not feasible computationally because of the extremely large memory and time requirements. A direct time domain numerical calculation for all of the cases considered also proved to be computationally challenging with our computer resources. The combined approach was determined to be computationally efficient, and it was validated with a few direct time domain simulations using CST's Microwave Studio.

We introduce the concept of the fidelity of a radiated output pulse to measure the likelihood that this pulse agrees with some ideal output pulse. For our discussion, we have selected the band-limited output pulse generated by the idealized infinitesimal dipole antenna, which is given in Fig. 2, to be that ideal pulse. The fidelity of any output pulse is calculated by the expression

$$\mathrm{FD}(\%) = 100 \times \mathrm{MAX}\left(\frac{s(t)}{||s(t)||} \otimes \frac{r(t)}{||r(t)||}\right) \tag{2}$$

where $s(t)$ is the idealized output signal, $r(t)$ is the actual output signal, $\otimes$ is the correlation operator, and $||\cdot||$ means to calculate the total signal power. For the output signal produced by the dispersive eight-element LPDA, which is shown in Fig. 4(b), the fidelity is 75.36%.

As pointed out in [5], when a broad bandwidth pulse is radiated by an LPDA antenna, its low frequency components are mainly radiated by the longer dipoles, which are located furthest from the feed point, while the higher frequencies are radiated by the shorter dipoles, which are located nearest that feed point. In addition, the longer dipoles are also further from the observation points in the main beam direction than the shorter ones are. These two facts combine to tell us that the time delay is larger in the low frequency regime and, consequently, there is more frequency dispersion introduced into the output pulse from that range.

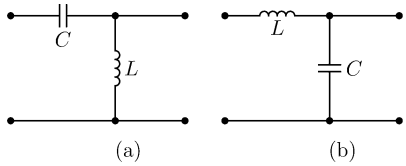

Fig. 5. (a) Left-hand phase-shifter, (b) right-hand phase-shifter.

III. MTM Phase Shifter Corrections

Based on these observations, we propose to use a set of electrically-small metamaterial-based phase shifters to adjust the time delays associated with each element, particularly at the low frequencies. As the currents propagate along a normal transmission line, they acquire a negative phase shift. The MTM phase shifter is essentially a left-handed transmission line; one cell of this left-handed transmission line structure is composed of a series capacitor C and a shunt inductor L as shown in Fig. 5(a). When the angular frequency $\omega \gg (1/2\sqrt{(LC)})$, this MTM phase shifter produces a positive phase shift given by the relation [6]

$$\Delta\phi \approx \frac{1}{\omega\sqrt{(LC)}}. \tag{3}$$

The set of MTM phase shifters introduced into the LPDA antenna is designed to produce the phase shifts, mod 2π, required to align the phases of all of the elements appropriately to achieve the desired time alignments. Both positive and negative phase shifters are actually necessary to achieve the desired phase compensation. A negative phase shift is simply obtained with a length of normal transmission line composed of shunt

capacitor C and a series inductor L as shown in Fig. 5(b). It must be noted, of course, that the positive phase shift $\Delta\phi$ in (3) can also be obtained by the negative phase shift $-(2\pi - \Delta\phi)$. Nonetheless, this would require introducing long segments of transmission line and, hence, would impact the balanced distribution of currents driving the radiating elements. The compactness of the MTM phase shifter is very attractive in this regards. Moreover, we have found that effective dispersion engineering in this LPDA case requires one to minimize the amount of phase shift associated with each radiating element to minimize the corresponding change in the magnitude of its current distributions.

Conceptually, we allow for the application of the MTM phase shifters along the transmission lines or at the feed points of the radiating elements. A diagram of the proposed modified LPDA antenna, including the MTM phase shifters, is shown in Fig. 6(a), where the blocks between the printed dipoles and the feed line represent the MTM-phase shifters. From the HFSS simulations of the performance of this MTM-phase shifter modified LPDA antenna, it was observed for a given dipole, with or without the phase shifter, that the current magnitude distribution remains essentially the same while the current phase is modified. For example, as shown in Fig. 6(b), the positive phase shift produced by an MTM-phase shifter is clearly shown. In this paper, the antenna performance is calculated using a MATLAB simulation model of the MTM-phase shifter modified LPDA antenna. For the designs considered below, we have restricted their location, because of the ease of construction of the required phase shifters, to the centers of the transmission line segments between the printed dipoles. In the MATLAB simulations, an MTM phase shifter is applied to the transmission line segment between every printed dipole; the current phase at the subsequent dipole is thus modified according to (3). The far zone electric field is then calculated according to (1).

For the purpose of comparison, we first give the ideal LPDA result in Fig. 7. For this case the phases $\phi_{f,n}$ of each of the current elements $I_{f,n}$ were artificially linearized with respect to the reference phase point of the LPDA, which was selected as explained below. In this manner, with respect to the far field phase in the endfire direction, the LPDA looks like a single element located at the phase reference point throughout the frequency range of interest. For this reason, this phase reference point is also referred to as the *equivalent radiation point* in this paper. The fidelity of this ideal LPDA output pulse was approximately 97%.

To determine the phase adjustment for each individual radiating element along the entire feed line of the LPDA antenna, we first choose a point along the feed line as the phase reference point and then find the phase shift for each element with respect to that reference point. The current phases are then artificially linearized with respect to it. In particular, for every antenna element, at its dominant frequency f_n, we find the phase shift for $I_{f_n,n}$ such that its phase is equal to the artificially linearized phase value relative to the reference value. This phase shift becomes the *target* phase shift for the nth antenna element. Then, all of the phase shifters are designed to achieve these target values at those frequencies. The phase shift values at the other frequencies follow from these design specifications. It should be noted that the current phase at other frequencies is usually not equal to the artificially linearized phase. As a result, there will be differences between the actual dispersion engineered LPDA antenna and the idealized linear phase shift version that generates the output waveform shown in Fig. 7. The output waveform is finally calculated. Further adjustments of the phase shifters are made to ensure both a good fidelity value and *target* phase shift values that are not too large so they can, in fact, be implemented physically.

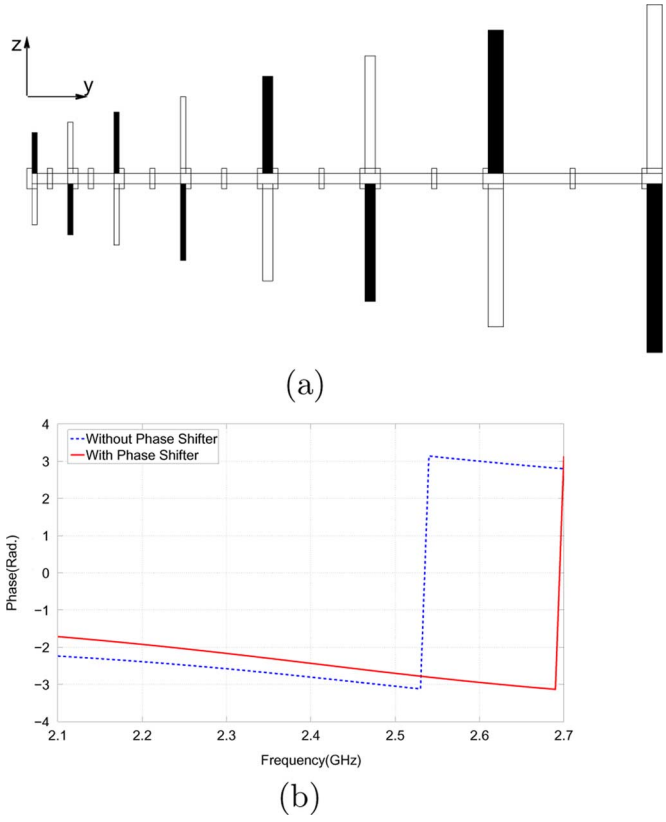

Fig. 6. Modified log-periodic antenna: (a) Geometry, (b) Original and modified phase of the current on a single dipole antenna.

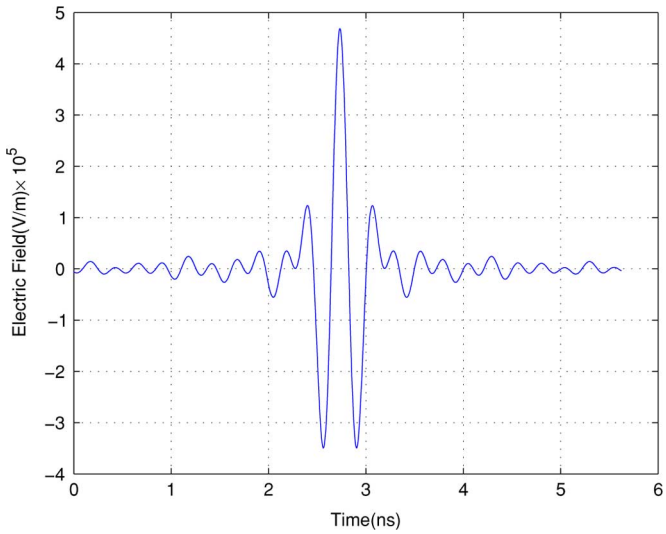

Fig. 7. Far-zone electric field with perfect phase compensation.

For the simulation results presented here, we choose the reference phase point as $((y_5+\lambda_{f_5}), 0, 0)$, where y_5 is the location of the fifth shortest antenna element and λ_{f_5} is the wavelength corresponding to the resonant frequency, f_5, of that element. Thus, for the LPDA arrays considered in this paper, we have elected to have the equivalent radiation point located at one of the radiating elements nearest to the center of the array. We note that with this choice, there is a closer agreement between the slopes of the response of the actual phase shifter and the linearized values not just at the dominant frequency, but also for neighboring frequencies as well.

Along the endfire direction, $(-\hat{y})$, the phases of all the elements in the far field are adjusted to the same point, i.e., to that reference phase point. We note that this phase adjustment is made only for this endfire (main beam) direction. If high fidelity were desired in a different direction that was supported by the patterns of each radiating element, the phase adjustments would then need to correspond to that direction. We also note that by electing to have the phase reference point near the middle of the array, the necessary phase shift magnitudes were minimized.

In the dispersion engineering procedure, we have also assumed that the current element magnitudes were fixed. However, the magnitude distributions of the currents along the array are, in fact, affected by the phase shifters because of the mutual couplings between the elements in the LPDA. These changes in the magnitudes of the currents are taken into account in our simulations. Phase shifters introducing large phase shifts change the magnitude distribution dramatically. For this reason, we basically could not always obtain the *target* phase adjustment without destroying the desired magnitude distribution. This was particularly true for the last adjustment made to the LPDA. After adjusting all of the previous elements, we found that some flexibility was needed in the choice of the last phase shift value to maximize the resulting fidelity. In addition to choosing the reference point to help minimize the size of the phase shifts, we also made the compromise to emphasize modifying the behavior of the longer elements; that is, the phase shifters were designed so that the phase adjustments for the longer antennas were matched to the *target* phase adjustment first rather than for the shorter antenna elements. Note that we also tried the obvious variation where the shorter antennas were emphasized first. It was discovered that because the phase variations are larger for the longer dipoles, the desired outcome was the best when the compensations for the dispersion behaviors of the longer dipole elements were achieved first. Moreover, we have found that even though we emphasize the longer elements first, the current distributions along the shorter elements nevertheless remain very close to their ideal counterparts.

The resulting far-zone electric fields for an eight element LPDA antenna and a ten element LPDA antenna are shown, respectively, in Figs. 8 and 9. The fidelity of the waveforms shown in Figs. 8(b) and 9(b) are 92.59% and 90.08%, respectively. One can see that the modified LPDA response is approaching the ideal result of 97% corresponding to Fig. 7. Details of the phase shifters we designed to achieve these results are given below. We note that while the modified current distributions do not fully recover the peak amplitude of the idealized output signal, they do reproduce a majority of the signal modulations well enough to achieve a high fidelity.

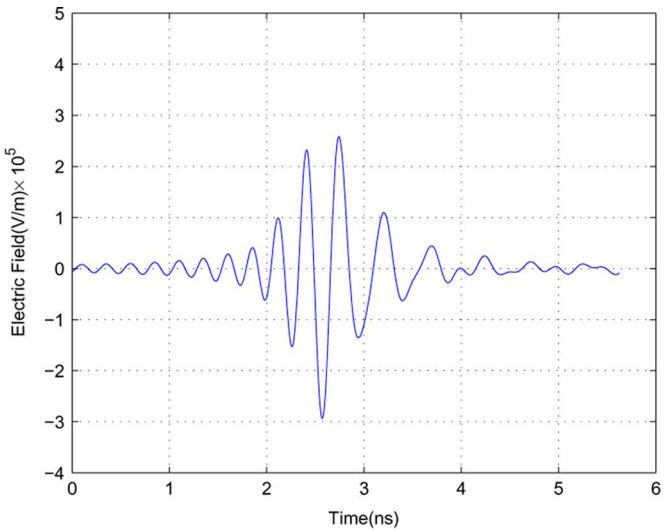

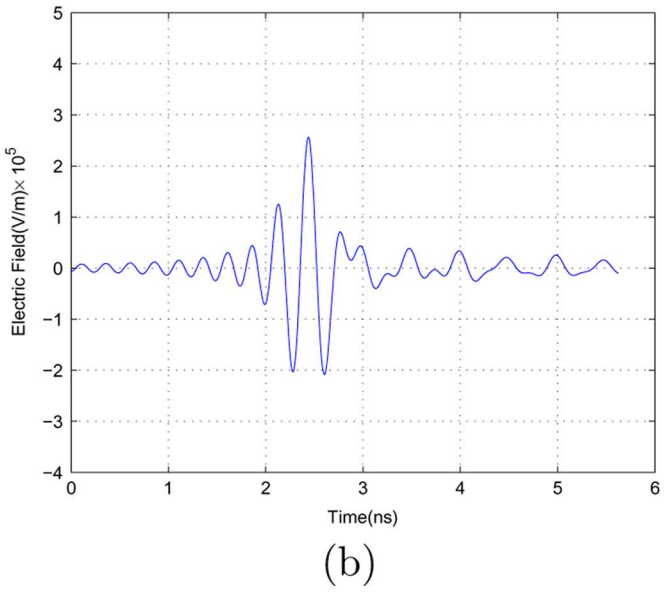

Fig. 8. Modified log-periodic eight element array output: (a) far-zone electric field without phase compensation, (b) far-zone electric field with designed phase compensation.

IV. MATLAB Simulations

The MATLAB simulator was used to obtain the desired phase shifts. These MATLAB simulations are based on the model Carrel introduced in [3] for the log-periodic cylindrical antenna shown in Fig. 10. Left-hand and right-hand phase-shifters are added to this model antenna as needed to obtain the desired phase compensated LPDA antenna. For the left-hand phase-shifter shown in Fig. 5(a), its $ABCD$ matrix is

$$\begin{bmatrix} A & B \\ C & D \end{bmatrix}_L = \begin{bmatrix} 1 & \frac{1}{j\omega C} \\ 0 & 1 \end{bmatrix} \begin{bmatrix} 1 & 0 \\ \frac{1}{j\omega L} & 1 \end{bmatrix} = \begin{bmatrix} 1-\frac{1}{\omega^2 LC} & \frac{1}{j\omega C} \\ \frac{1}{j\omega L} & 1 \end{bmatrix}. \quad (4)$$

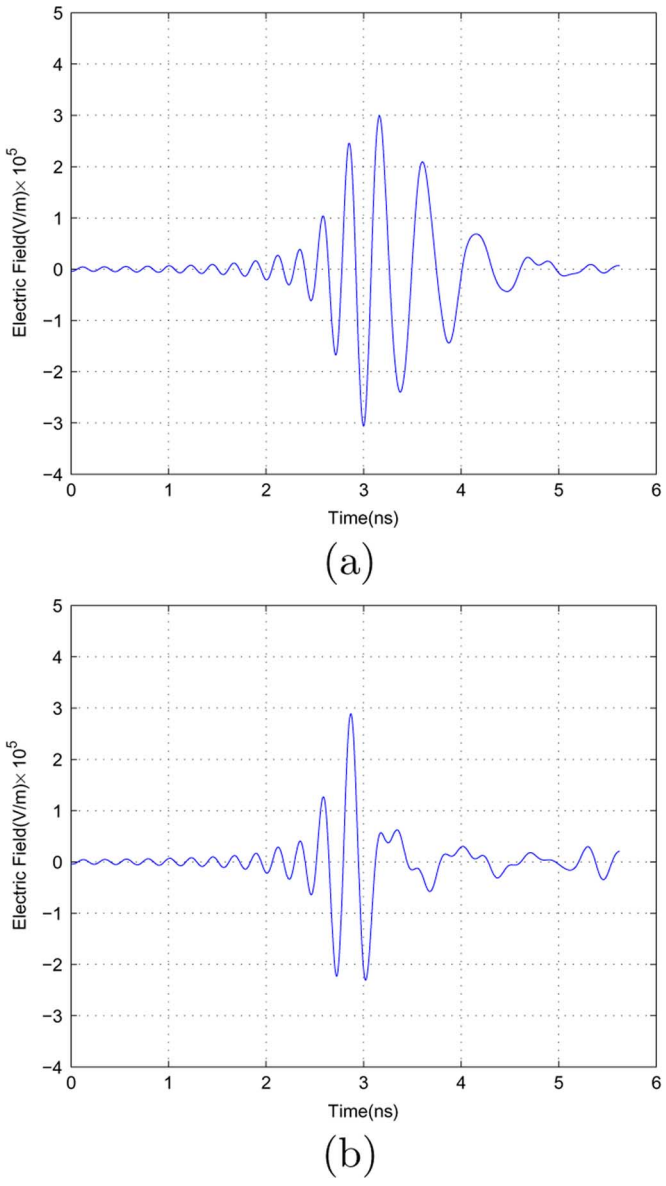

Fig. 9. Modified log-periodic 10 element array output: (a) far-zone electric field without phase compensation and (b) far-zone electric field with designed phase compensation.

Similarly, for the right-hand phase-shifter shown in Fig. 5(b), its $ABCD$ matrix is

$$\begin{bmatrix} A & B \\ C & D \end{bmatrix}_R = \begin{bmatrix} 1 & j\omega L \\ 0 & 1 \end{bmatrix} \begin{bmatrix} 1 & 0 \\ j\omega C & 1 \end{bmatrix} = \begin{bmatrix} 1-\omega^2 LC & j\omega L \\ j\omega C & 1 \end{bmatrix}. \quad (5)$$

The phase-shifter between the $(n-1)$th and nth elements of the LPDA antenna is added at the middle of the transmission line of length l_n that connects those two elements as shown in Fig. 13. The $ABCD$ matrix representation of this phase-shifter modified transmission line is

$$\begin{bmatrix} A_n & B_n \\ C_n & D_n \end{bmatrix} = \begin{bmatrix} \cos\left(\beta\frac{l_n}{2}\right) & jZ_0 \sin\left(\beta\frac{l_n}{2}\right) \\ jY_0 \sin\left(\beta\frac{l_n}{2}\right) & \cos\left(\beta\frac{l_n}{2}\right) \end{bmatrix} \begin{bmatrix} A_p & B_p \\ C_p & D_p \end{bmatrix} \times \begin{bmatrix} \cos\left(\beta\frac{l_n}{2}\right) & jZ_0 \sin\left(\beta\frac{l_n}{2}\right) \\ jY_0 \sin\left(\beta\frac{l_n}{2}\right) & \cos\left(\beta\frac{l_n}{2}\right) \end{bmatrix} \quad (6)$$

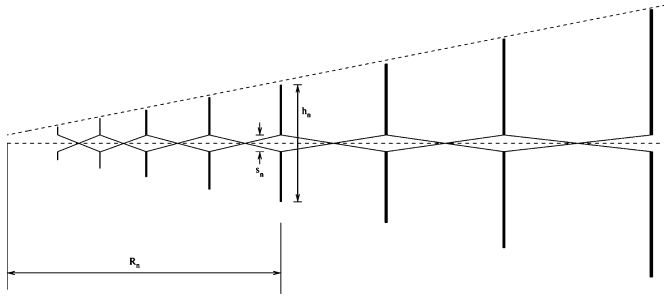

Fig. 10. Log-Periodic cylindrical antenna.

where

$$\begin{bmatrix} A_p & B_p \\ C_p & D_p \end{bmatrix}$$

is the matrix that represents the phase-shifter, and Z_0 and Y_0 are the characteristic impedance and admittance, respectively, of the transmission line. Referring to Fig. 13, for the phase shifter between the $(n-1)$th and nth radiating element, the relation between the input voltage and current of the phase shifter, respectively, V_{n-1} and I''_{n-1}, and its output voltage and current, respectively, V_n and I'_n, are

$$\begin{bmatrix} V_{n-1} \\ I''_{n-1} \end{bmatrix} = \begin{bmatrix} A_n & B_n \\ C_n & D_n \end{bmatrix} \begin{bmatrix} V_n \\ I'_n \end{bmatrix}. \quad (7)$$

Equation (7) can be rearranged in the form

$$I'_n = \frac{1}{B_n} V_{n-1} - \frac{A_n}{B_n} V_n$$
$$I''_{n-1} = \frac{D_n}{B_n} V_{n-1} + \left(C_n - \frac{A_n D_n}{B_n} \right) V_n. \quad (8)$$

Then, according to Fig. 13, the current I_n applied to the nth radiating element is given by the expression

$$\begin{aligned} I_n &= I''_n - I'_n \\ &= -\frac{1}{B_n} V_{n-1} + \left(\frac{A_n}{B_n} + \frac{D_{n+1}}{B_{n+1}} \right) V_n \\ &\quad + \left(C_{n+1} - \frac{A_{n+1} D_{n+1}}{B_{n+1}} \right) V_{n+1}. \end{aligned} \quad (9)$$

Because of the crisscross connections of the LPDA feed line, when n is odd, $Vt_n = V_n$ and $It_n = I_n$, and when n is even, $Vt_n = -V_n$ and $It_n = -I_n$, where Vt_n and It_n are, respectively, the voltage and current at the terminals of the nth antenna. Thus the current at the terminals of the antenna, (9), can then be written in the form

$$\begin{aligned} It_n &= \frac{1}{B_n} Vt_{n-1} + \left(\frac{A_n}{B_n} + \frac{D_{n+1}}{B_{n+1}} \right) Vt_n \\ &\quad + \left(-C_{n+1} + \frac{A_{n+1} D_{n+1}}{B_{n+1}} \right) Vt_{n+1}. \end{aligned} \quad (10)$$

For $n = 1$ and $n = N$, the terminal currents are explicitly

$$It_1 = I''_1 = \frac{D_2}{B_2} Vt_1 + \left(-C_2 + \frac{A_2 D_2}{B_2} \right) Vt_2$$
$$It_N = \frac{1}{B_N} Vt_{N-1} + \left(\frac{1}{Z_L} + \frac{A_N}{B_N} \right) Vt_N \quad (11)$$

TABLE I
PHASE-SHIFTER PARAMETERS VALUES FOR THE EIGHT ELEMENT LPDA ANTENNA

n	Type&Number	$C(pF)$
1	N	N
2	N	N
3	R,1	0.03
4	L,1	9
5	R,1	0.14
6	R,3	0.14
7	R,4	0.27
8	R,4	0.44

TABLE II
PHASE-SHIFTER PARAMETERS VALUES FOR THE TEN ELEMENT LPDA ANTENNA

n	Type&Number	$C(pF)$
1	N	N
2	L,1	50
3	R,1	0.011
4	L,1	4.4
5	N	N
6	R,3	0.18
7	R,3	0.32
8	R,4	0.4
9	R,4	0.47
10	R,4	0.65

where Z_L is the terminating impedance of the LPDA antenna. The admittance matrix $[Y_T]$ of the LPDA antenna driven with the phase shifter modified transmission lines can be derived immediately from (10) and (11). The currents on the radiating elements, needed to calculate the far field output pulse, are then obtained from the relation

$$\bar{I}_A = [Y_A]\{([Y_T] + [Y_A])^{-1}\bar{I}\} \tag{12}$$

where $[Y_A]$ is the admittance matrix of the radiating elements and $\bar{I}$ is the current source driving the LPDA antenna as defined in [3]. The MATLAB simulations of the far-field output waveform generated by the dispersion engineered LPDA antenna were then calculated with (1) using the feed point currents, $I_{f,n}$, i.e., the elements of the array, $\bar{I}_A$.

As noted previously, for ease of fabrication of the dispersion engineered LPDA antenna, only phase shifters located in the middle of transmission lines were used, as described above. The formulation, which includes phase shifters applied directly to the radiating elements, is summarized for completeness in the Appendix. The transmission-line-based phase shifters were designed to dispersion engineer both the eight element and ten element LPDA antennas. The parameters that define the phase-shifters introduced in each case to achieve the highest fidelity values are listed, respectively, in Tables I and II, where n means the nth antenna, the C column gives the capacitor values used in the phase-shifters, and the *Type & Number* column gives the number of phase-shifters and whether they are right-hand (R) or left-hand (L). The corresponding inductor values are determined for each phase-shifter by the expression

$$L = Z_0^2 C \tag{13}$$

TABLE III
EIGHT ELEMENT LOG-PERIODIC ANTENNA DIMENSIONS

n	τ	σ	R_{max}(mm)	h_{max}(mm)	LD
8	0.867	0.152	157.7	138	117

TABLE IV
TEN ELEMENT LOG-PERIODIC ANTENNA DIMENSIONS

n	τ	σ	R_{max}(mm)	h_{max}(mm)	LD
10	0.867	0.152	198.9	174	117

where $Z_0 = 77.23\,\Omega$ is the characteristic impedance of the feed line in a dipole-based LPDA antenna. The dimensions of the dipole LPDA antenna shown in Fig. 10 are given explicitly in Tables III and IV for each of the cases considered here, where $\tau = (R_n/R_{n+1}) = (h_n/h_{n+1})$ and $\sigma = (R_{n+1} - R_n/2h_n)$. In Tables III and IV, $h_{\max}$ is the length of the longest antenna, $R_{\max}$ is the distance between the longest antenna and the terminating apex. The gap, s_n, between the feed lines is set to a constant value: $s_n = 2.159$ mm. The diameter of each transmission line segment is set to 1.778 mm. The diameter d_n of the nth dipole antenna is determined by $d_n = h_n/LD$, where LD is the ratio of the length of that dipole to its diameter. The LPDA antenna is assumed to be fed at the shortest antenna; it is terminated with a matched resistor, i.e., $Z_L = 73\,\Omega$.

As noted above, the performance of the dispersion engineered LPDA antenna was measured by the fidelity of the bandlimited actual output waveform with respect to the bandlimited reference output waveform generated by the idealized infinitesimal dipole antenna. Taking into account the total power normalizations of the actual and reference output signals, the fidelity of the actual output waveform is a measure of how well the bandlimited ideal derivative of the bipolar input pulse is recovered. For the eight element antenna, the result was bandlimited to the interval $1.0\ \text{GHz} \leq f \leq 4.0$ GHz. On the other hand, for the ten element antenna, because of its broader bandwidth, the excitation pulse was band limited to the frequency interval: $0.5\ \text{GHz} \leq f \leq 4.5$ GHz. To ensure a large tolerance factor in the results for any future fabrication and measurement efforts, this 4.0 GHz frequency bandwidth was larger than the desired operating interval of $1.723\ \text{GHz} \leq f \leq 4.06$ GHz. We note that there is a significant increase in the phase offset as the number of elements in an LPDA antenna is increased. This was the main reason that we studied both the eight and ten element LPDA antennas in detail. Similar fidelity improvements were realized with LPDA antennas with even more elements.

For the configurations specified by Tables I and II, the required phase-shifts are given in Table V. The output waveforms with and without these designed phase compensations are shown, respectively, in Figs. 8 and 9. For the eight element antenna, the fidelity was 73.39% without phase compensation and 92.6% with phase compensation. For the 10 element antenna, the fidelity was 65.73% without phase compensation and 90.08% with phase compensation. These fidelity results hold for all observation points in the endfire direction as long as those points are in the far field of the entire LPDA. Note the decrease of the fidelity of the output waveform between the uncompensated ten and eight element systems. If more bandwidth is desired, more elements have to be added to an

TABLE V
PHASE SHIFTS AT THE DOMINANT RADIATION FREQUENCIES

n	Eight Elemant		Ten Element	
	Freq.(GHz)	Phase-shift(Rad)	Freq.(GHz)	Phase-shift(Rad)
1	4.0	-0.1048	3.85	-0.1939
2	4.0	-0.0694	4.43	-0.0276
3	3.85	-0.1815	4.1	-0.0853
4	3.32	0.1244	3.59	0.2597
5	2.94	-0.0984	3.11	0.4896
6	2.62	-0.2273	2.77	0.0124
7	2.28	-1.6479	2.38	-1.2438
8	1.98	3.1633	2.04	4.0648
9			1.8	-4.1377
10			1.52	1.3999

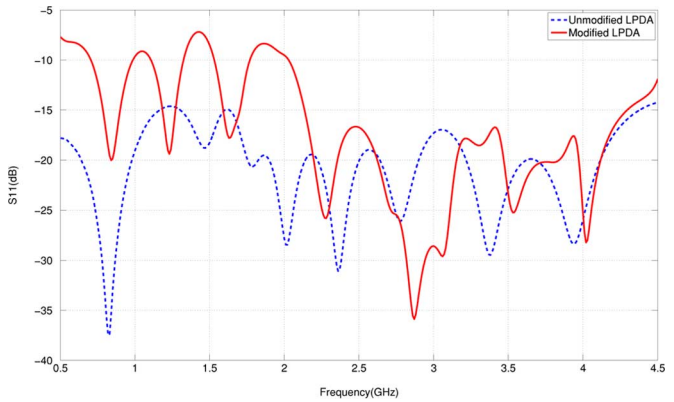

Fig. 11. The S_{11} values for the dispersion-engineered 10 element LPDA as a function of the frequency.

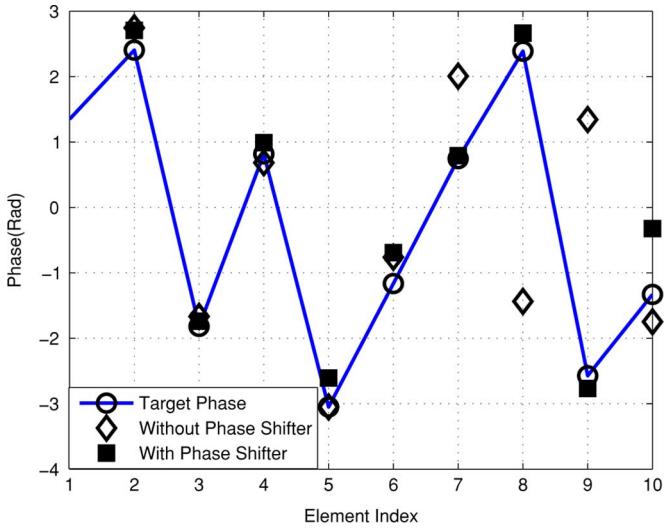

Fig. 12. The phase distribution along the dispersion-engineered 10 element LPDA.

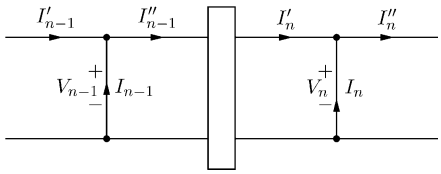

Fig. 13. Phase-shifter in transmission line.

LPDA antenna. As more elements are added, the dispersion effects become larger. While the introduction of the MTM phase shifters produces a significant improvement in the fidelity of the output waveform even for a modest number of radiating elements, the improvement becomes even more significant as the number of elements is increased.

For the dispersion compensated and uncompensated 10 element LPDAs we show, respectively, in Figs. 11 and 12, the S_{11} values over the frequency band of interest and their phase values in comparison to the corresponding values in the ideal linearized case. According to the S_{11} values, the dispersion compensated 10 element LPDA still has a wide bandwidth even though the impact of the introduction of the phase shifters at the lower frequencies is noticeable, particularly at the resonant frequencies of the radiating elements for which the phase shifters were designed. This maintenance of the bandwidth is further confirmed by the overall fidelity of the output signal. On the other hand, the small drop in the peak amplitude of the modified LPDA's output time signal in comparison to the ideal result is attributable to this small increase in the insertion losses caused by the presence of the phase shifters at the lower frequencies. The impact on the phase distribution achieved by introducing the phase shifters along the LPDA is clearly seen in Fig. 12. The phase distribution is matched to the target phases, particularly in the low frequency range, except for the last element, which, as noted above, requires some flexibility in its phase value to optimize the overall fidelity.

It should be noted that the fidelity in (2) could also have been defined as

$$\mathrm{FD}(\%) = 100 \times \mathrm{MAX}\left(\left|\frac{s(t)}{\|s(t)\|} \otimes \frac{r(t)}{\|r(t)\|}\right|\right). \qquad (14)$$

By adding the magnitude operator (i.e., the $|\cdot|$), this definition would allow a sign difference between the signals $s(t)$ and $r(t)$, that is, it would allow for the introduction of an extra π phase shift. Such a π phase shift could occur, for instance, if one elected to feed the LPDA antenna differently. Based on this magnitude definition, the fidelities of the pulses without phase adjustment in Figs. 8(a) and 9(a) are 85.03% and 68.50%, respectively. There would be no changes in the fidelity values associated with the dispersion compensated LPDA antenna results since they have the correct signs already. However, because our dispersion engineering is focussed on phase compensation, we elected to emphasize (2) in our results, i.e., (2) more accurately accounts for all of the differences in the phases between the actual and reference output pulses.

Representative E-plane antenna patterns produced by the modified LPDA and by the unmodified LPDA at 2.04 GHz, 3.59 GHz, and 4.5 GHz, are shown, respectively, in Fig. 14(a)–(c). As seen in Fig. 14(a), it was found that without the additional tweaking to achieve a high fidelity, the modified LPDA does not maintain the requisite endfire antenna pattern originally obtained in the low frequency range. On the other hand, the antenna patterns shown in Fig. 14(b) and (c) show that it does in the mid and high frequency ranges. The optimum solution, which was based on the best obtainable value of the

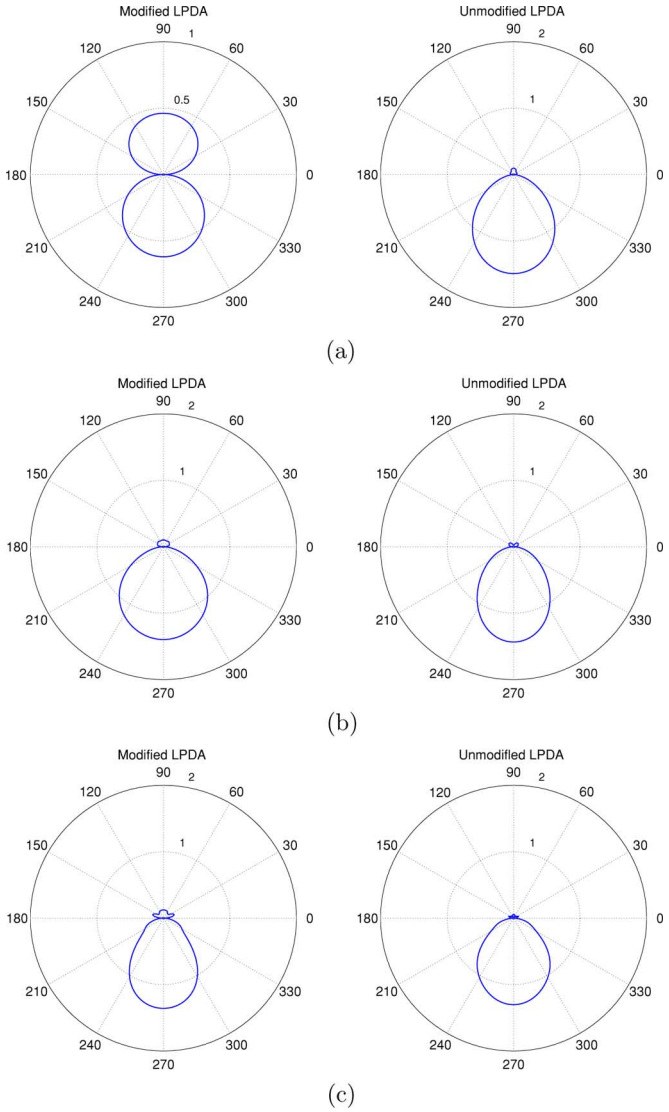

Fig. 14. Modified LPDA and Unmodified LPDA E-Plane Antenna Patterns. (a) 2.04 GHz, (b) 3.59 GHz, (c) 4.5 GHz.

time domain fidelity value, does recover the desired endfire antenna patterns throughout the frequency range of operation. The reason that the basic modified LPDA failed to maintain this highly desirable frequency domain antenna pattern property in the low frequency range is that although the current phase was adjusted to the optimum solution value at each of the resonant frequencies, at other frequencies, the differences between the phases of the modified LPDA and the optimum solution were significant, particularly in the lower frequency range. By further adjusting the phase values to achieve a broader matching of the responses, the endfire radiation pattern behavior was recovered over the operational band.

The phase reference point or the equivalent radiation point is a simple approach to understand the optimum solution. To find the equivalent radiation point in the far field main beam direction, we define an equivalent current for the LPDA to be

$$I_{\text{equv}} = \sum_{n=1}^{N} \alpha_n I_n e^{-jkd_n} = |I_{\text{equv}}| e^{-j(kd+\phi_0)} = |I_{\text{equv}}| e^{-j\phi_{\text{equv}}} \tag{15}$$

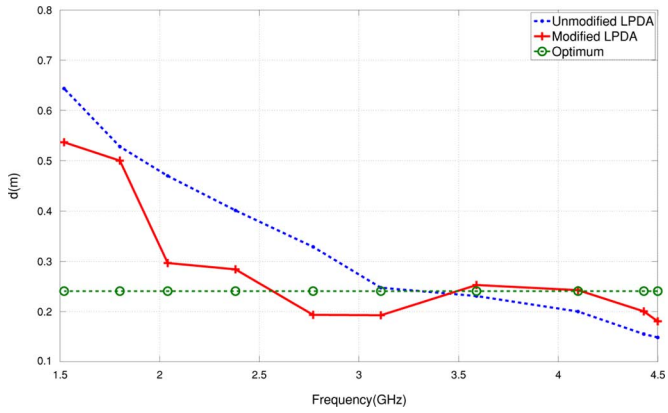

Fig. 15. Phase center locations.

where

$$\alpha_n = \frac{1}{\sin(kl_n)} \frac{\cos\left(\frac{kl_n}{2}\cos(\theta)\right) - \cos\left(\frac{kl_n}{2}\right)}{\sin(\theta)} \tag{16}$$

is the current amplitude weighted dipole element pattern function, l_n is the length of the nth element, and d_n is the distance between the nth antenna and the apex point, the apex point being taken to be the coordinate system origin. This equivalent current is to be understood as the single current source which generates the LPDA far field at the observation point at a specific frequency.

This source is located at the "equivalent radiation point", a distance d from the apex, and has a relative initial phase ϕ_0 with respect to it. It should be noted that in general the equivalent radiation point is different from the usual phase center concept. The phase center is an equivalent phase reference point at a given frequency that is defined by the curved wavefront that passes through the far field observation point. However, it can be proved that in the main beam direction, the radiation point and the phase center coincide. Since the fidelity is obtained for the output pulse in the main beam (endfire) direction relative to the idealized output pulse in the same direction, the phase center and the equivalent radiation point coincide for our dispersion engineering application.

The phase center calculation for the optimum solution shows that its phase center does not change with respect to the frequency, i.e., a fixed equivalent radiation point is obtained for the optimum solution. Thus, it can be used as a reference to describe the phase evolution in the main beam direction. Consequently, according to (15), the equivalent radiation point distance and, hence, the phase center at each frequency of interest can be calculated as

$$d = \frac{d\{\phi_{\text{equv}}\}}{d\{f\}} / (2\pi c) \tag{17}$$

where c is the light speed in vacuum. The calculated phase centers for the unmodified and the modified LPDAs are shown in Fig. 15. They are compared there to the fixed point value of the optimum solution. Fig. 15 illustrates that as the frequency changes, the phase centers of the modified LPDA vary less from the optimum solution value than the original LPDA antenna phase centers do. Thus, the dispersion engineering reduces the

phase center variation from the optimum solution. In particular, the variance from the optimum solution values of the phase centers for the modified LPDA is 0.164, while it is 0.288 for the original unmodified LPDA. This is yet another confirmation that the modified LPDA is indeed approaching the optimum solution.

V. Conclusion

In this paper, we have demonstrated that the frequency dispersion associated with an LPDA antenna can be improved by applying left-hand and right-hand phase shifters to adjust the relative phases of the radiating elements to achieve a better time alignment of the individual frequency components. The improvement was measured by comparing the fidelity of the dispersion-engineered LPDA antenna's far field output pulse to an idealized output pulse generated by driving an infinitesimal dipole with the input excitation current pulse. The performance characteristics of the dispersion-engineered LPDA antenna were obtained with MATLAB and HFSS simulations. In the MATLAB simulations, the LPDA antenna model reported in [3] was extended in this paper to accommodate the MTM-based phase shifters. The procedures to find the suitable phase shifters, both in the transmission lines between the radiating elements and at the terminals of the radiating elements, were provided. Significant improvements in the output pulse fidelity were achieved for a dispersion-engineered LPDA antenna with a large number of elements.

The HFSS simulations were performed for an eight element printed dipole LPDA antenna. The frequency dispersion associated with an LPDA antenna is readily observed in its output pulse. Because of the high complexity of these simulations, the MATLAB simulations were performed rather using a known cylindrical dipole LPDA antenna model. In particular, the MATLAB simulator was applied to the phase-shifter modified eight element LPDA antenna and the ten element LPDA antenna with and without phase shifters. We note that, as is pointed out in [4], the printed dipole and cylindrical dipole can be made to be equivalent. In fact, in both the HFSS and MATLAB simulations for the eight element LPDA antenna without phase shifters, we obtain currents whose magnitudes and phases are very similar to each other. Thus, we have found that the MATLAB simulation results using an appropriately designed cylindrical dipole LPDA antenna are very consistent with those generated by the equivalent printed dipole LPDA antenna HFSS simulations.

Appendix
Phase Shifters Included on the Radiating Elements

In Section IV, we calculated the admittance matrix $[Y_T]$ for the transmission-line-based phase shifters. As noted, we can also add phase shifters at the connection between the antenna elements and the transmission line. In this case, the admittance matrix $[Y_A]$ for the element must be calculated. For a phase shifter added to the nth antenna, the relation between its input voltage V_n' and current I_n' and its output voltage V_n and current I_n is

$$\begin{bmatrix} V_n' \\ I_n' \end{bmatrix} = \begin{bmatrix} A_n & B_n \\ C_n & D_n \end{bmatrix} \begin{bmatrix} V_n \\ I_n \end{bmatrix}. \tag{18}$$

Then, one has immediately

$$\begin{aligned} \begin{bmatrix} V_n \\ I_n \end{bmatrix} &= \frac{1}{A_nD_n - B_nC_n} \begin{bmatrix} D_n & -B_n \\ -C_n & A_n \end{bmatrix} \begin{bmatrix} V_n' \\ I_n' \end{bmatrix} \\ &= \begin{bmatrix} A_n' & B_n' \\ C_n' & D_n' \end{bmatrix} \begin{bmatrix} V_n' \\ I_n' \end{bmatrix}. \end{aligned} \tag{19}$$

In [3], the antenna voltage vector, $\bar{V_A}[V_1, V_2, \cdots, V_n]^{\mathrm{T}}$, and the antenna current vector, $\bar{I_A} = [I_1, I_2, \cdots, I_n]^{\mathrm{T}}$, are related by the expression

$$\bar{I_A} = [Y_A]\bar{V_A} \tag{20}$$

where $[Y_A]$ is the admittance matrix of the radiating element. According to (19)

$$\begin{aligned} \bar{V_A} &= \mathbf{A}'\bar{V}' + \mathbf{B}'\bar{I}' \\ \bar{I_A} &= \mathbf{C}'\bar{V}' + \mathbf{D}'\bar{I}' \end{aligned} \tag{21}$$

where the matrices $\mathbf{A}', \mathbf{B}', \mathbf{C}', \mathbf{D}'$ are diagonal, their diagonal elements being the terms A_n', B_n', C_n', and D_n' give in (19), respectively. The relation between $\bar{V}'$ and $\bar{I}'$ after the phase-shifter is added can then be calculated as

$$\mathbf{C}'\bar{V}' + \mathbf{D}'\bar{I}' = [Y_A](\mathbf{A}'\bar{V}' + \mathbf{B}'\bar{I}'). \tag{22}$$

Rearranging (22), one obtains

$$\bar{I}' = (\mathbf{D}' - [Y_A]\mathbf{B}')^{-1}([Y_A]\mathbf{A}' - \mathbf{C}')\bar{V}' = [Y_A']\bar{V}' \tag{23}$$

where $[Y_A']$ is the admittance matrix of the phase shifter-modified radiating elements. The output waveform follows immediately with the MATLAB simulator.

References

[1] R. W. Ziolkowski and P. Jin, "Using metamaterials to achieve phase center compensation in a log-periodic array," in *Proc. IEEE Antennas Propag. Society Int. Symp.*, Hawaii, 2007, pp. 3461–3464.

[2] A. Paul and I. Gupta, "An analysis of log periodic antenna with printed dipoles," *IEEE Trans. Microw. Theory Tech.*, pp. 114–117, 1981.

[3] R. L. Carrel, "Analysis and design of the log-periodic dipole antenna," Ph.D. dissertation, UIUC, , 1976.

[4] C. Balanis, *Antenna Theory*, 3rd ed. Hoboken, NJ: Wiley, 2006.

[5] C. M. Knop, "On transient radiation from a log-periodic dipole array," *IEEE Trans. Antennas Propag.*, pp. 807–808, 1970.

[6] C. Caloz and T. Itoh, *Electromagnetic Metamaterials*. Hoboken, NJ: Wiley, 2006.

Richard W. Ziolkowski (M'97–SM'91–F'94) received the Sc.B. degree in physics (*magna cum laude* with honors) from Brown University, Providence, RI, in 1974 and the M.S. and Ph.D. degrees in physics from the University of Illinois at Urbana-Champaign, in 1975 and 1980, respectively.

He was a member of the Engineering Research Division, Lawrence Livermore National Laboratory, CA, from 1981 to 1990 and served as the Leader of the Computational Electronics and Electromagnetics Thrust Area for the Engineering Directorate from 1984 to 1990. He joined the Department of Electrical and Computer Engineering, University of Arizona, Tuscon, as an Associate Professor in 1990, was promoted to Full Professor in 1996, and was selected by the Faculty to serve as the Kenneth Von Behren Chaired Professor, for 2003 to 2005. He currently is serving as the Litton Industries John M. Leonis Distinguished Professor. He holds a joint appointment with the College of Optical Sciences at the University of Arizona. His research interests include the application of new mathematical and numerical methods to linear and nonlinear problems dealing with the interaction of acoustic and electromagnetic waves with complex media, metamaterials, and realistic structures.

Prof. Ziolkowski is a member of Tau Beta Pi, Sigma Xi, Phi Kappa Phi, the American Physical Society, the Optical Society of America, the Acoustical Society of America, and Commissions B (Fields and Waves) and D (Electronics and Photonics) of the International Union of Radio Science (URSI). He was awarded the Tau Beta Pi Professor of the Year Award in 1993 and the IEEE and Eta Kappa Nu Outstanding Teaching Award in 1993 and 1998. He served as the Vice Chairman of the 1989 IEEE/AP-S and URSI Symposium in San Jose, and as the Technical Program Chairperson for the 1998 IEEE Conference on Electromagnetic Field Computation. He was an Associate Editor for the IEEE TRANSACTIONS ON ANTENNAS AND PROPAGATION from 1993 to 1998. He served as a member of the IEEE Antennas and Propagation Society (AP-S) Administrative Committee (ADCOM) from 2000 to 2002. He served as the IEEE AP-S Vice President in 2004 and President in 2005. He is currently serving as a Past-President member of the AP-S ADCOM. He was a Steering Committee Member for the 2004 ESA Antenna Technology Workshop on Innovative Periodic Antennas. He served as a co-Chair of the International Advisory Committee for the inaugural IEEE International Workshop on Antenna Technology: Small Antennas and Novel Metamaterials, IWAT2005, and as a member of the International Advisory Committee for IWAT 2006 and 2007. He was a member of the International Advisory Committee for the IEEE 2005 International Symposium on Microwave, Antenna, Propagation and EMC Technologies, MAPE2005. He served as an Overseas Corresponding Member of the ISAP2007 Organizing Committee. He was a Co-Guest Editor for the October 2003 IEEE TRANSACTIONS ON ANTENNAS AND PROPAGATION Special Issue on Metamaterials. For the US URSI Society he served as Secretary for Commission B (Fields and Waves) from 1993 to 1996 and as Chairperson of the Technical Activities Committee from 1997 to 1999, and as Secretary for Commission D (Electronics and Photonics) from 2001 to 2002. He served as a Member-at-Large of the U.S. National Committee (USNC) of URSI from 2000 to 2002 and is now serving as a member of the International Commission B Technical Activities Board. He is a Fellow of the Optical Society of America. He was a Co-Guest Editor of the 1998 special issue of the *Journal of the Optical Society of America A* featuring Mathematics and Modeling in Modem Optics. He was a Co-Organizer of the Photonics Nanostructures Special Symposia at the 1998, 1999, 2000 OSA Integrated Photonics Research (IPR) Topical Meetings. He served as the Chair of the IPR sub-committee IV, Nanostructure Photonics, in 2001.

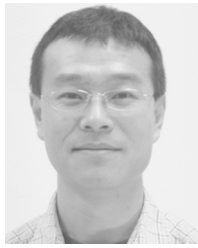

Peng Jin (S'05) received the B.Sc. degree from the University of Science and Technology of China, HeiFei, China, in 1999 and the M.Sc. degree from North Dakota State University, Fargo, in 2003. Currently, he is working toward the Ph.D. degree at the University of Arizona, Tucson.

His research interest include electrically small antennas, metamaterials applications on antenna design.